The Effect of Tidal Power Generation on Sediment Transport in Muskeget Channel

1.0 SWATH Bathymetry Survey and Analysis

Overview

A high resolution bathymetric survey of Muskeget channel and surroundings was completed in fall of 2010 (Denny et al., 2012). The chief survey scientist was Jane Denny from the USGS Woods Hole Science Center (WHSC). Rich Signell (USGS, WHSC) helped coordinate the survey design. The survey was conducted using an interferometric sonar unit which can measure bathymetry along a swath on either side of the ship track with a width of roughly seven times the water depth. The goals of the survey were to obtain a baseline high resolution bathymetry dataset for Muskeget Channel, characterize the large scale bedforms in the Channel surroundings, and characterize the bedforms in the vicinity of the two potential routes by which the installation would be connected with Marthas Vineyard.

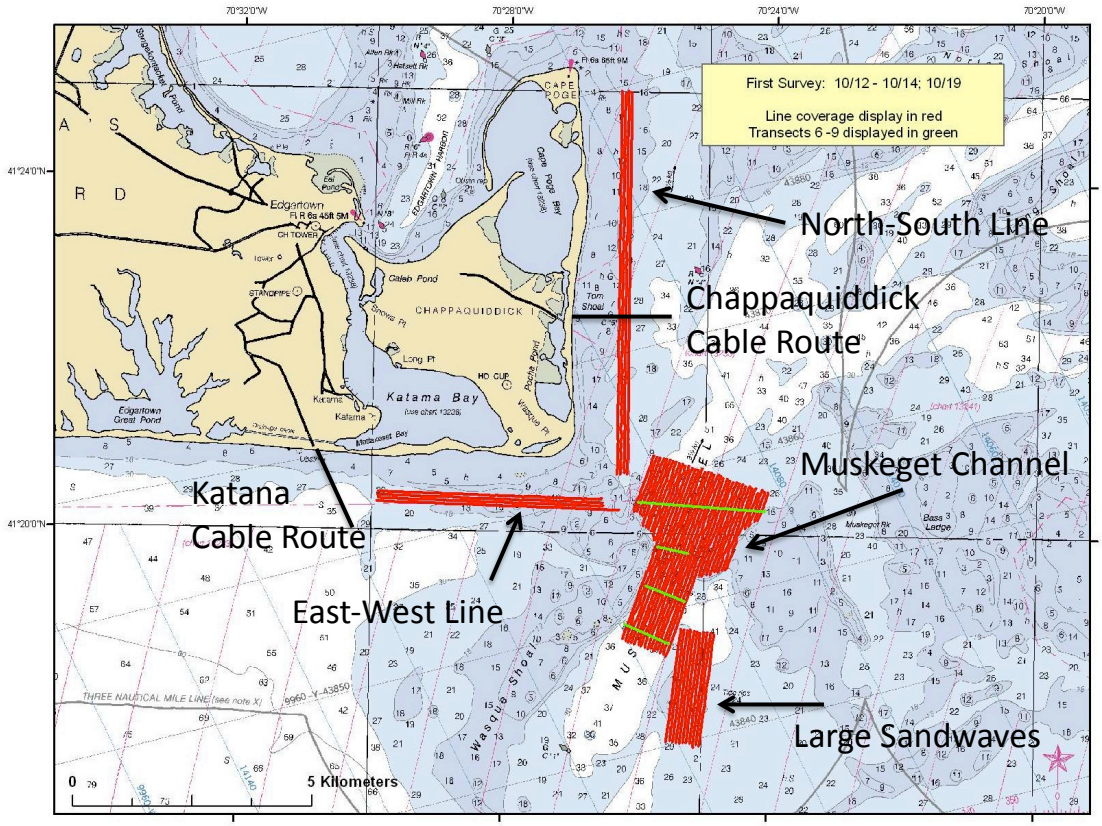

Figure III-1: USGS SWATH Bathymetry Survey Design

Survey Design

The first survey was conducted from 10/12/2010-10/14/2010. The survey included the main channel, a region containing large sandwaves to the south of the channel, and two sections along the eastern and southern shores of Marth's vineyard in the vicinity of the two proposed cable connections (Fig. III-1). The second survey was completed in a single day on 11/16/2010. Due to survey constraints, only the areas containing large sand waves and the two cable route transects were re-surveyed. The resulting data provides a monthly snapshot at these three locations. A DGPS-RTK was used for navigation and to adjust for tides. The data was projected to the local state plane, gridded at 1-m resolution, and is available for download or access through opendap capable software on a USGS Thredds server at: http://geoport.whoi.edu/thredds/dodsC/usgs/data0/muskeget/.

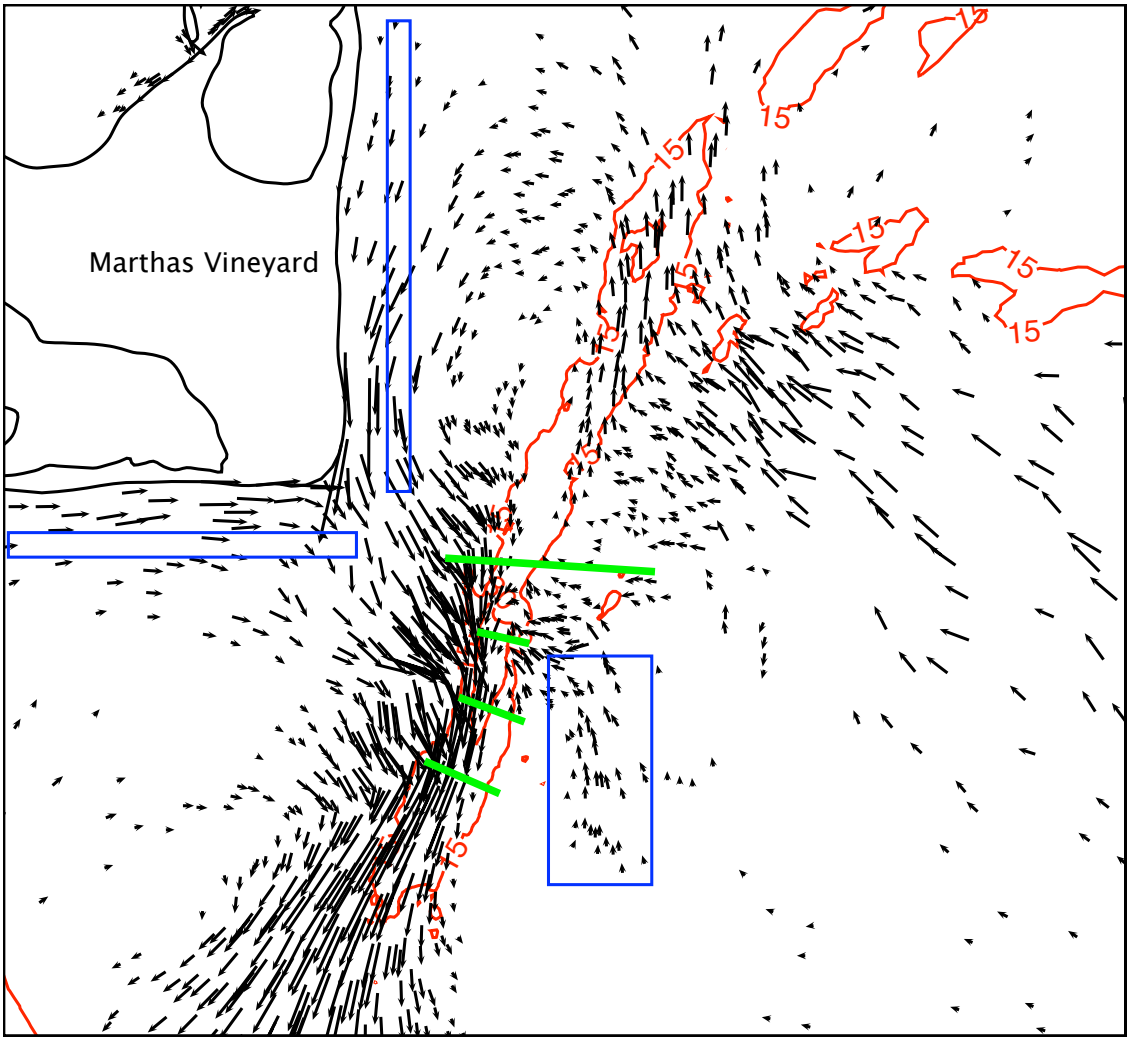

Figure III-2: Model-computed vertically-averaged tidal residual flow vectors for M_2 boundary forcing. SMAST Coastal Systems Program ADCP Transects 6-9 (green lines) and 15-m isobath shown for reference. Blue boxes: Approximate locations of Large Sandwaves, East-West Line and North-South Line of USGS SWATH bathymetry survey (ref: Fig III-1).

Characterization of Bedforms

Muskeget Channel

The deepest part of Muskeget Channel (Figure III-3) contains a series of fairly symmetric rolling bedforms of roughly 5-m height and 100-m wavelength. These large bedforms are most closely located to transects 7 and 8 of the SMAST Coastal Systems Program ADCP Survey. These transects also show the most promise for TKE extraction (ORPC, 2010). Given the extremely high shear stresses and mobility of the local dominant substrates these bedforms should be re-surveyed to assess potential impact on structures, stays, and cable routes. The bedform characteristics and fan extending in the direction of the strong residual current are reminiscient of the well studied bedforms of San Francisco Bay.

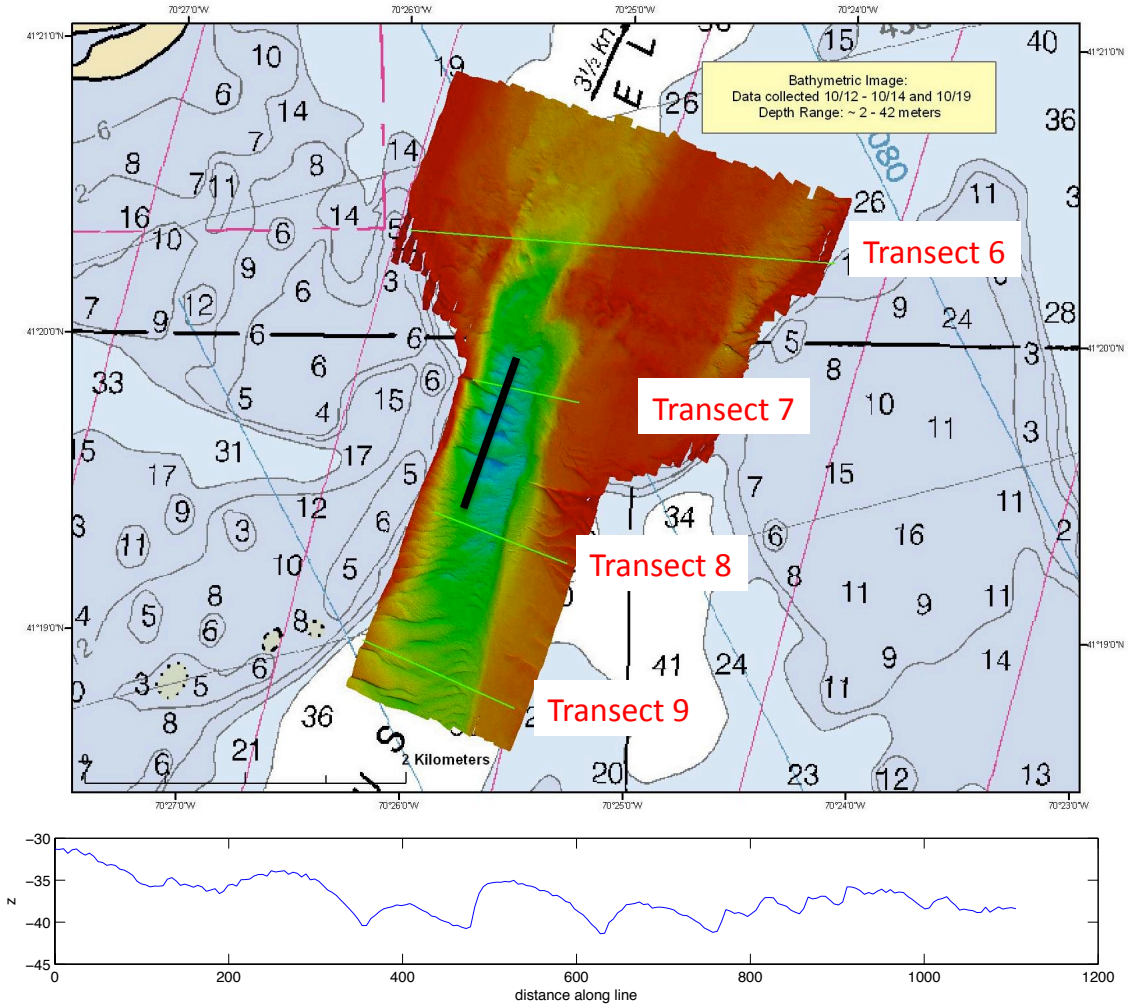

Figure III-3: Upper: Bathymetry of Muskeget Channel derived from the USGS SWATH Bathymetry Survey. SMAST Coastal Systems Lab ADCP Transects 6-9 (green lines) shown for reference. Lower: topographic profile (m) along the main channel (black line) from SW to NE.

Large Amplitude Sand Waves

The large amplitude sand waves (Figure III-4) have an average wavelength of 225m and an average height of 4.5m. The average upstream slope is .025 and average slip face slope is .08. They are of similar scale to the well-studied sand waves in the Bay of Fundy. Their ratio of height to wavelength falls within two well-known relationships derived from the Bay of Fundy data (Figure III-7). While the tidal residual flow in the main Muskeget Channel is predominantly to the south (Figure III-2), the large amplitude sandwaves lie off the main channel in an area with weak northward residual flow.

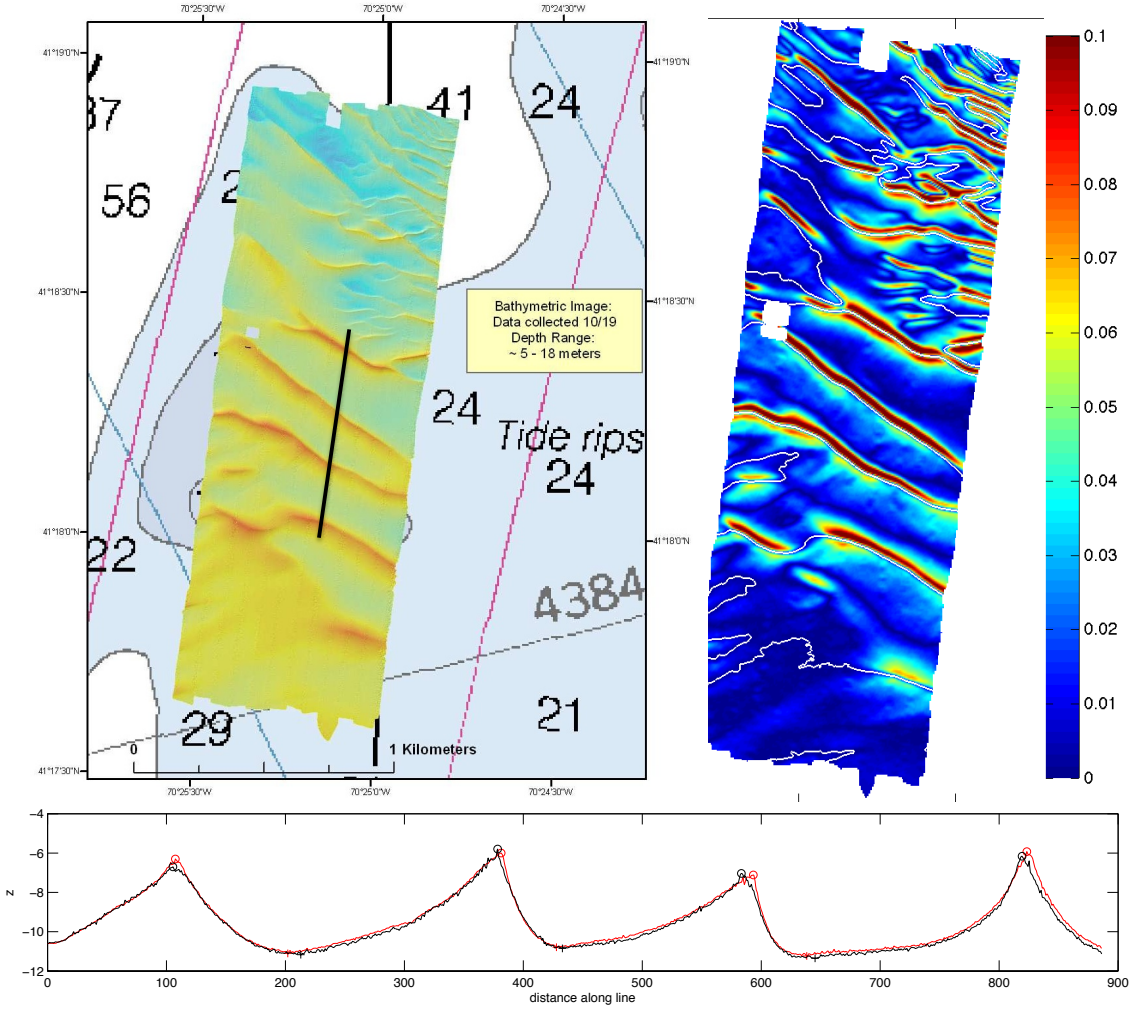

Figure III-4: Upper left: Bathymetry of large sand waves derived from the USGS Muskeget SWATH Bathymetry Survey. Upper right: Bed slope (m/m) and location of wave crests (white lines) for the large sand wave field south of Muskeget Channel. Lower: bed profile normal to wave crests [ref: black line in upper left figure] from South to North. [Red: survey 1, Black: survey 2]

The large sand waves have a clear slip face oriented towards the North which is consistent with the direction of this residual current. If the same transect is taken through the second survey (one month later), crests have moved an average of 5m towards the south. Based on crest motion this would imply a net motion of 17 cm/day which is similar in magnitude to migration speeds in the Bay of Fundy. However, the profile indicate that the slip face is becoming less steep and that the crest motion is more likely a result of the sand wave relaxing rather than a rigid translation of a fixed waveform.

North-South survey

The North-South survey bisects the proposed route of the Chappaquidick cable route and thus is useful for determining the necessary dredge depth. Sandwaves along the N-S transect can be divided into two groups. The northern group are roughly 90m in length and 0.7 m in height and have slip faces oriented to the north. The southern group are shorter with a mean wavelength of 40-m and height of 0.8m. This group has a reversed orientation with the slip face on the south side. The slip face orientation of the southern group is also more clearly defined.

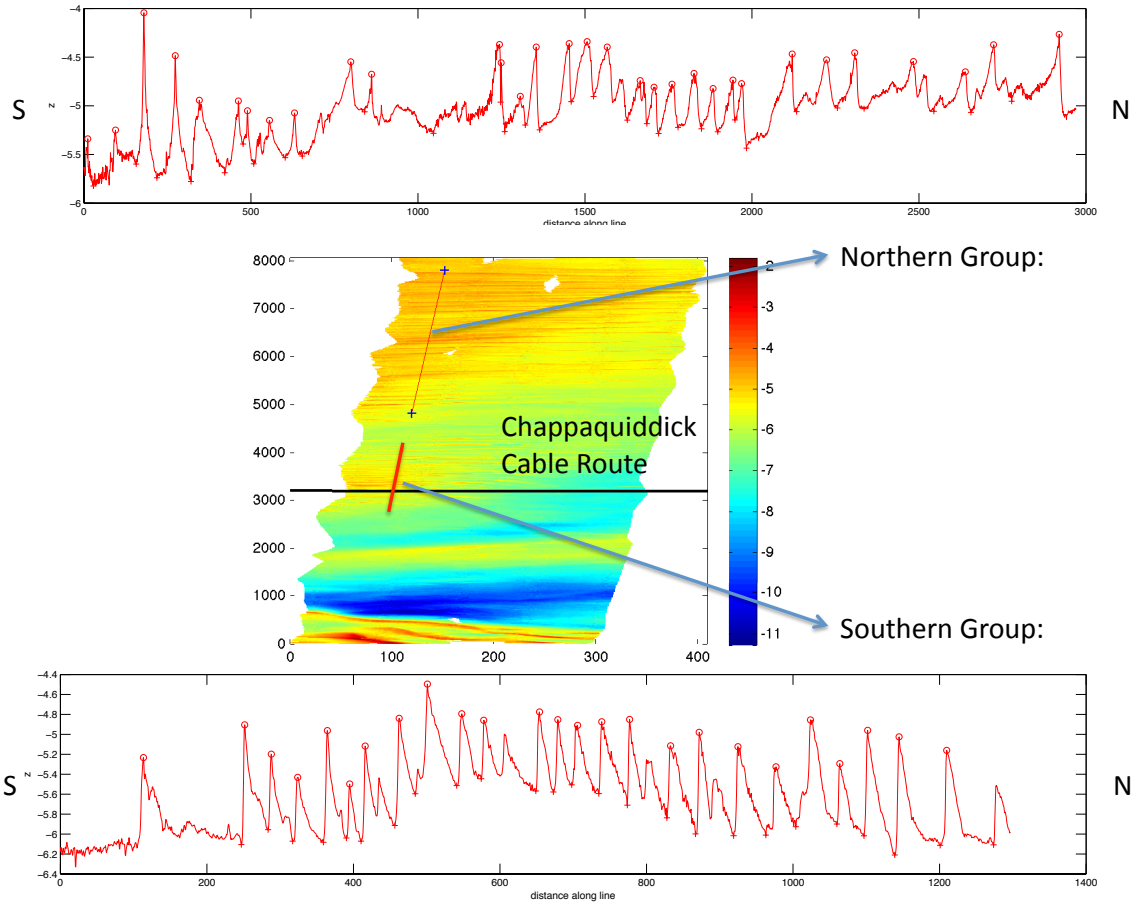

Figure III-5: Upper: bathymetric profile (m) from south to north normal to wave crests in the northern group of bedforms east of Chappaquiddick (ref: thin red line in central panel). Center: bathymetry along North-South line of SWATH Bathymetry Survey (ref

Fig: III-1). Bottom: bathymetric profile (m) from south to north normal to crests in the southern group of bedforms east of Chappaquiddick (ref: thick red line in central panel).

The proposed Chappaquiddick cable route intersects the southern group. Based on the model-computed residual currents (Figure III-2), the tidally-driven flow is predominantly southward in the nearshore region of the east-facing portions of Chappaquiddick. The magnitude of the residual current increases towards the Southeast point of Marthas Vineyard.

East-West survey

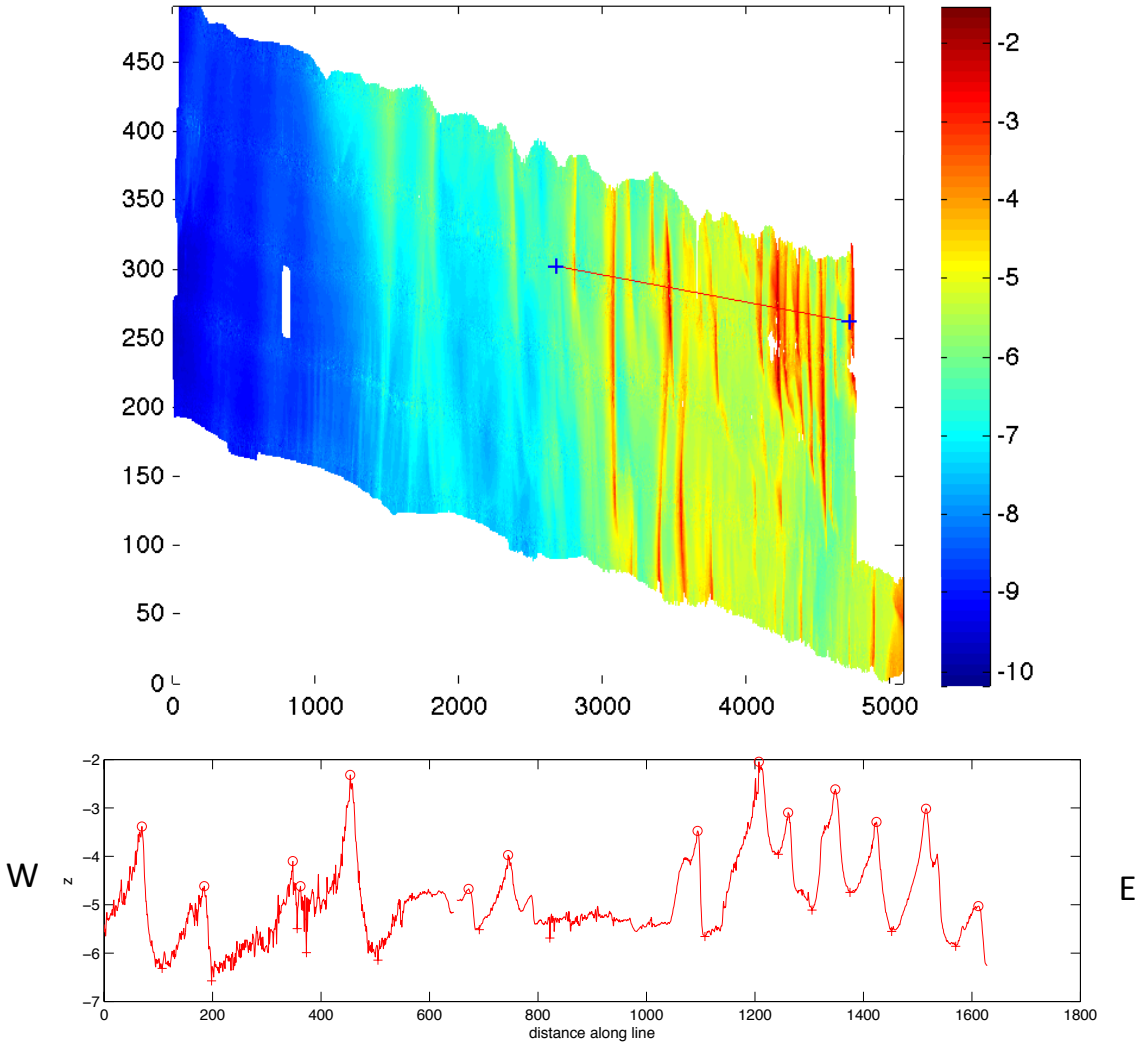

Figure III-6: Upper: bathymetry along East-West line of USGS SWATH Bathymetry Survey (see Fig: III-1). Bottom: bathymetric profile (m) from west to east normal to wave crests south of Katama Bay (ref: red line in upper fig).

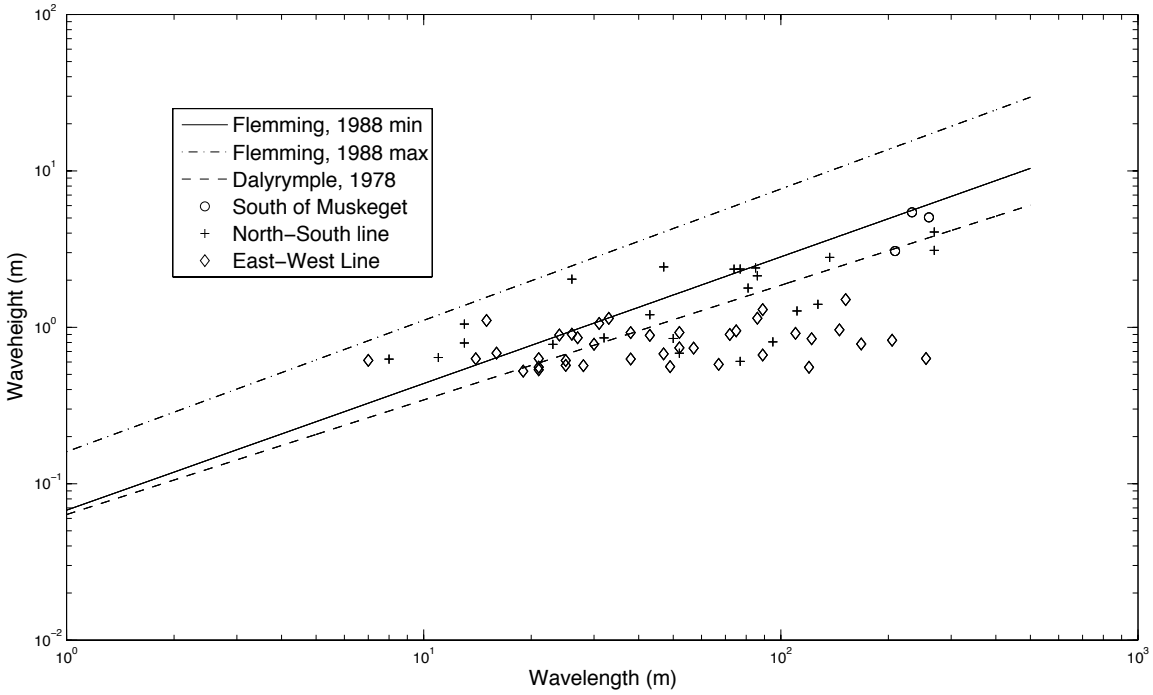

Figure III-7: Comparison of bedform characteristics in the vicinity of Muskeget Channel with wave height – wavelength relationships from empirical relationships.

The bedforms along the E-W survey have a mean wavelength of 120m and height of 2m. The slip face is to the east which corresponds with the residual flow direction (Fig. III-2). These sandwaves are occuring roughly 3km to the east of the proposed Katama cable route. An inlet to Katama Bay was created during the Patriots Day storm (April, 2007) and may have some influence on the formation of bedforms in this region through both modifications to hydrodynamic forcing and potentially sediment supply (R. Geyer, P. Traykovski, personal communication). The inlet is migrating eastward.

2.0 Impact Modelling Studies

Approach

Hydrodynamic Model

FVCOM is a Fortran90 software package for the simulation of ocean processes in coastal regions (Chen et al., 2003, 2006; Cowles, 2008). The publicly available model has a growing user base and has been employed in a wide variety of applications. The kernel of the code computes a solution of the hydrostatic primitive equations on unstructured grids using a finite-volume flux formulation. The unstructured grid modeling approach is highly advantageous for resolving dynamics in regions with complex shorelines and bathymetry such as the Massachusetts coastal region (Fig. III-8). The horizontal spatial fluxes are discretized using a second-order accurate scheme (Kobayashi, 1999). For the vertical discretization, a generalized terrain-following coordinate is employed. FVCOM is interfaced to the General Ocean Turbulence Model (GOTM) libraries to provide an array of turbulence closure schemes including the standard Mellor-Yamada 2.5 and k-epsilon approaches. An explicit mode splitting technique is used to integrate the model forward in time (Madala and Piascek, 1977). In this method, the barotropic (vertically-homogenous) mode is integrated separately from the baroclinic motion using the shorter time steps required by the gravity wave speed. The baroclinic (three-dimensional) mode can be stepped at a time step constrained by the maximum internal wave speed. In a general application, this results in approximately a ten-fold increase in the allowable stable time step. The model is fully parallelized using a Single Program Multiple Data (SPMD) approach (Cowles, 2008). Message passing is programmed using the Message Passing Interface (MPI) standard using non-blocking sends and receives. The parallelized code scales well on modern machines, is highly portable to numerous architectures, and greatly increases the capabilities of the original core scheme by extending practical model simulation timescales and spatial resolution.

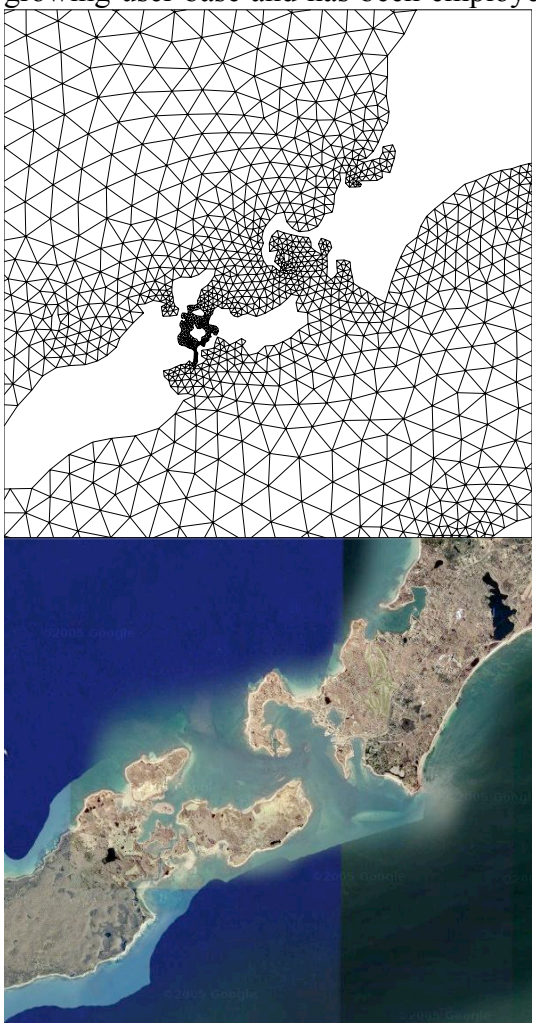

Figure III-8: FVCOM mesh near Woods Hole, MA

Sediment Model

The FVCOM Sediment model is based on the Community Sediment Transport Modeling System (CSTMS) (http://www.cstms.org) as implemented in the Regional Ocean Modeling System (ROMS) (Warner et al, 2006). The model includes transport of both the suspended load and bedload. The number of sediment classes is flexible, and for each class, parameters such as critical shear stress, mean diameter, and settling velocity must be defined. Complex bed dynamics are included with a user-prescribed number of layers defined by the layer number, fractions of each sediment class, an age, and a thickness. Due to sharp gradients in the concentration profile that can occur near the bottom, a flux-limited scheme is used in FVCOM for the settling equation. This scheme introduces antidiffusion by means of a minmod limiter and maintains second order spatial accuracy away from extrema. The bedload is treated using the MPM (Meyer-Peter and Müeller, 1948) scheme to calculate the local load and fluxes from the bed are then determined by calculating the divergence of the local load.

Turbine Parameterization

To model the impact of the turbines on the fluid we use a volumetric subgridscale parameterization. The momentum loss in the water column due to the device is given by

$$S_u = \frac{1}{2} C_p A_{dev} \rho U^2 \qquad \text{(Eq. III-1)}$$

where C_p is the hydrodynamic efficiency of the device, A_{dev} is the effective cross sectional area, $U = U(x,y,z)$ is the fluid velocity, and ρ is the fluid density. This term is added to the three-dimensional x- and y-direction momentum equations as a sink term. This approach has been used successfully in wake studies of wind turbines (Réthoré et al., 2010).

Model Setup

Domain and Bathymetry

The model domain includes the entirety of the Massachusetts Coastal waters (Fig. III-9). The coastline was based on a high resolution product developed by the Massachusetts Coastal Zone Management. The Bathymetry is a composite set which incluced the USGS 3-Arc Second Gulf of Maine database complemented by the NOAA 1/3 Arc-second Nantucket Inundation DEM in the southern portions of Nantucket Sound and the USGS Muskeget SWATH Bathymetry in the main Muskeget Channel. The mesh is locally refined in the vicinity of Muskeget Channel for the purpose of capturing the spatial complexity of the currents in the impact studies. A sequence of three models were developed providing coarse, medium, and fine resolution (Table III-1). This enabled more rapid model development and a formal assessment of grid independence in the results of the impact studies.

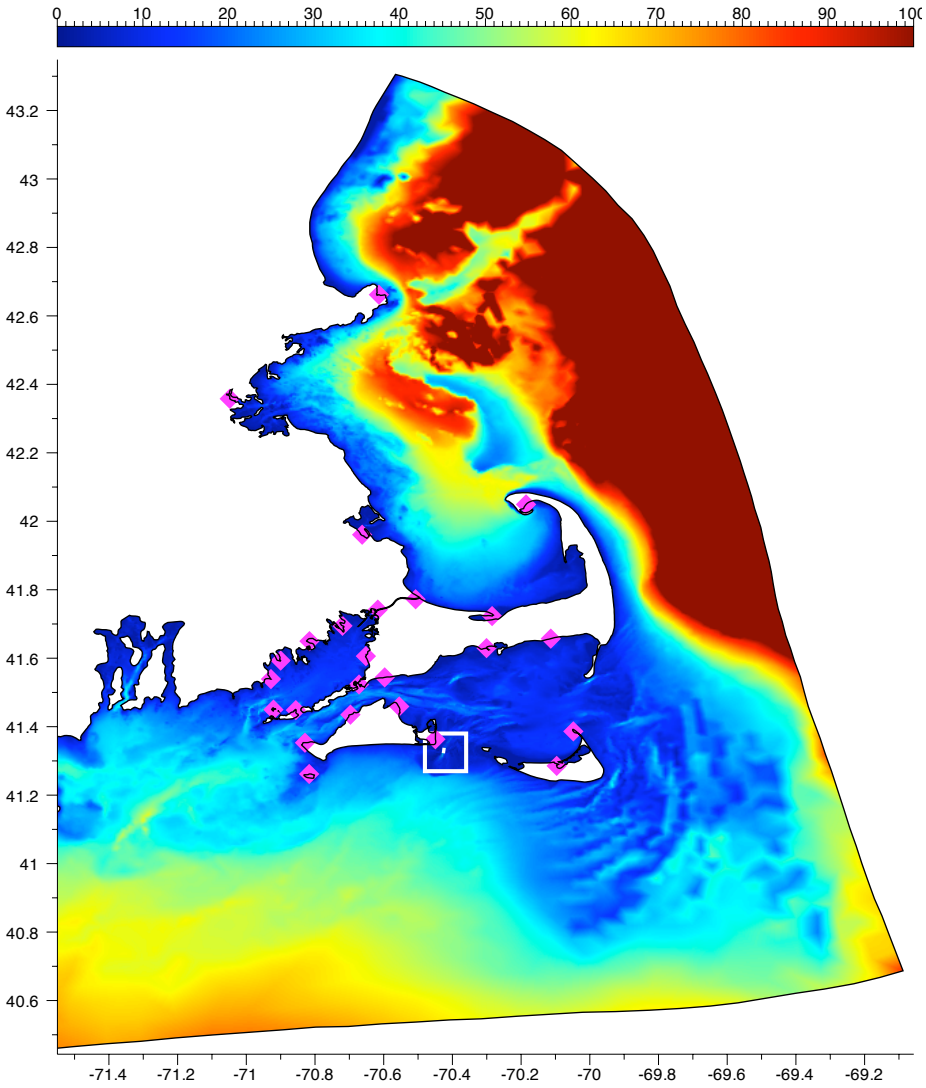

Figure III-9: Domain and bathymetry (m) for the Mass Tidal Model (MTM) series. Muskeget region (white box) and tidal harmonics observation sites shown for reference.

Forcing

The model is forced at the open boundary using 6 tidal constituents [M_2,S_2,N_2,O_1,K_1,M_4]. These consitituents were extracted from a large scale tidal model (Chen et al., 2011) and adjusted to improve the harmonic response of sea surface elevation with the domain.

Model	#Elements	Resolution (m) [Muskeget/Coastal]	Time Step (s)	T_{month} @ 100 Gflop
mtm-4	60K	150 / 100	10	10 hours
mtm-2	120K	70 / 50	5	50 hours
mtm-1	285K	30 / 25	2.5	100 hours

Table III-1: Specifications of Mass Tidal Models

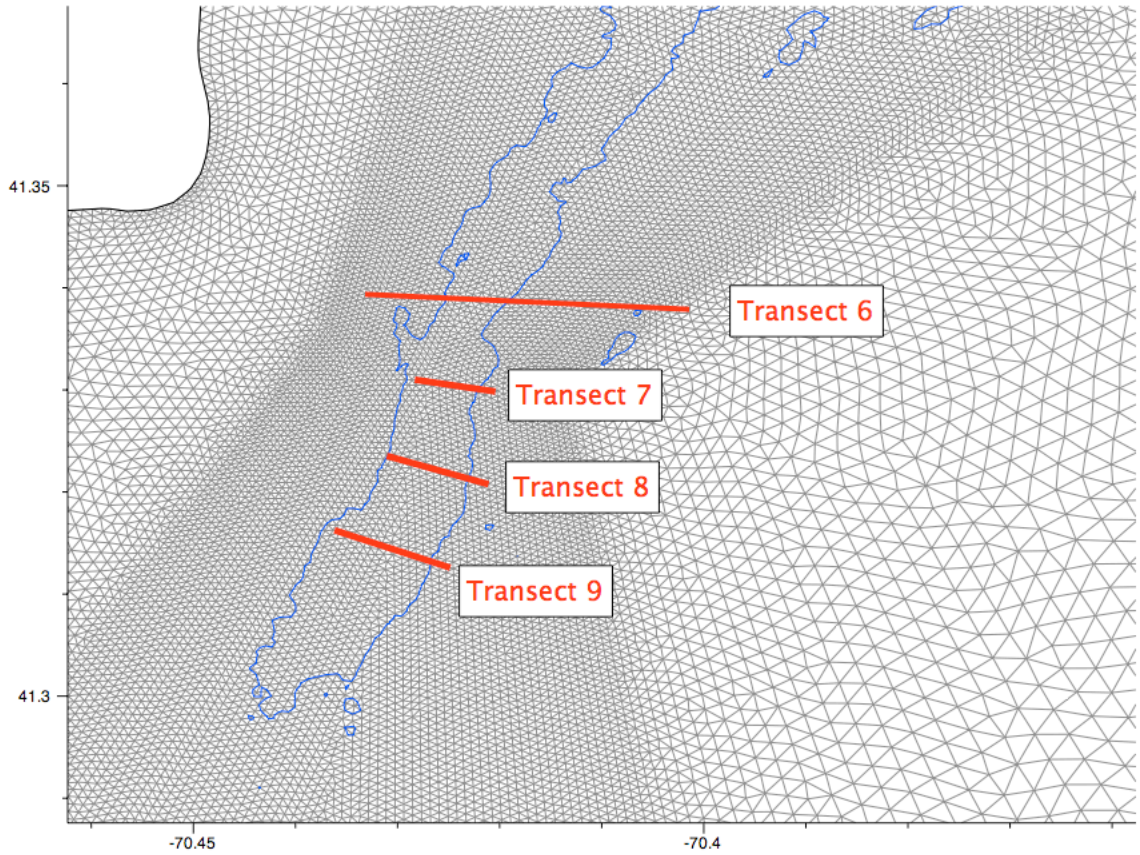

Figure III-10: FVCOM model mesh in the vicinity of Muskeget Channel with ADCP Transects from SMAST Coastal Systems Lab ADCP survey. 15-m isobath shown for reference (blue line).

Model Validation

Tidal Harmonics and Mean Annual Power Density

Tidal harmonics at 24 stations are used to validate the five principal components (M_2,S_2,N_2,K_1,O_1) as well as the principal overtide M_4. The tidal dynamics south of the Cape are complex owing to the prominent convergence of two large scale tidal waves, one approaching from the Gulf of Maine through the Great South Channel and the other propagating across the New England Shelf (Chen et. al, 2011). Capturing the correct phase and amplitude requires accurate forcing and a model that can resolve properly the coastline and small-scale bathymetric features. Standard deviations of model-computed and observed amplitude and phase differences are 1.45 cm and 6.1° for M_2, .85 cm and 3.1° for N_2, 0.6 cm and 11.0° for S_2, 2.6 cm and 3.2° for K_1, and 1.7 cm and 6.5° for O_1. Measurement uncertainty is provided at only a few stations and thus it is not possible to determine if the model-observation differences are within the range.

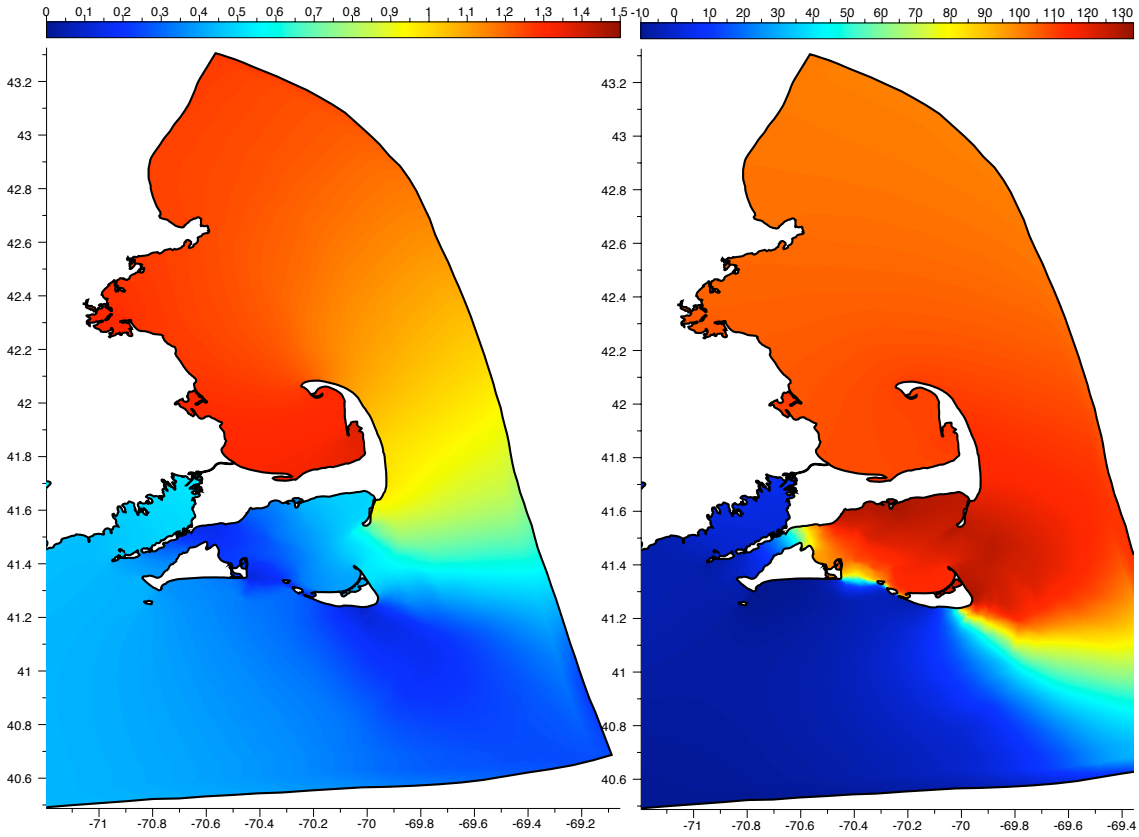

Figure III-11: M_2 Amplitude (m) [left figure] and phase (°G) [right figure] computed using the FVCOM mtm-1.

ADCP Transects

The model-computed velocity fields through transects 6-9 were compared with measurements made by the SMAST Coastal Systems Program (provided by B. Howes). These measurements were made during large spring tide in June, 2009. The model was run over the same period as the measurements using 6 components of tidal forcing at the boundary (M_2,S_2,N_2,K_1,O_1,M_4). The model captures well the magnitude of the currents (Figure III-12a-d) and is able to resolve the complex structure of the flow in the channel. During flood the peak velocity resides in the east part of the channel and during ebb, it shifts towards the central and western edge of the channel. This is evident at both transects 7 in the deeper portion of the Channel and transect 9 in the shallower regions near the southern extent of Muskeget Channel. There is significant vertical shear in both the observed and model-computed velocity fields. Optimal placement of turbines will likely require working within exclusion constraints from navigation, minimizing loading from survey waves while trying to capture as much of the greater power near the surface.

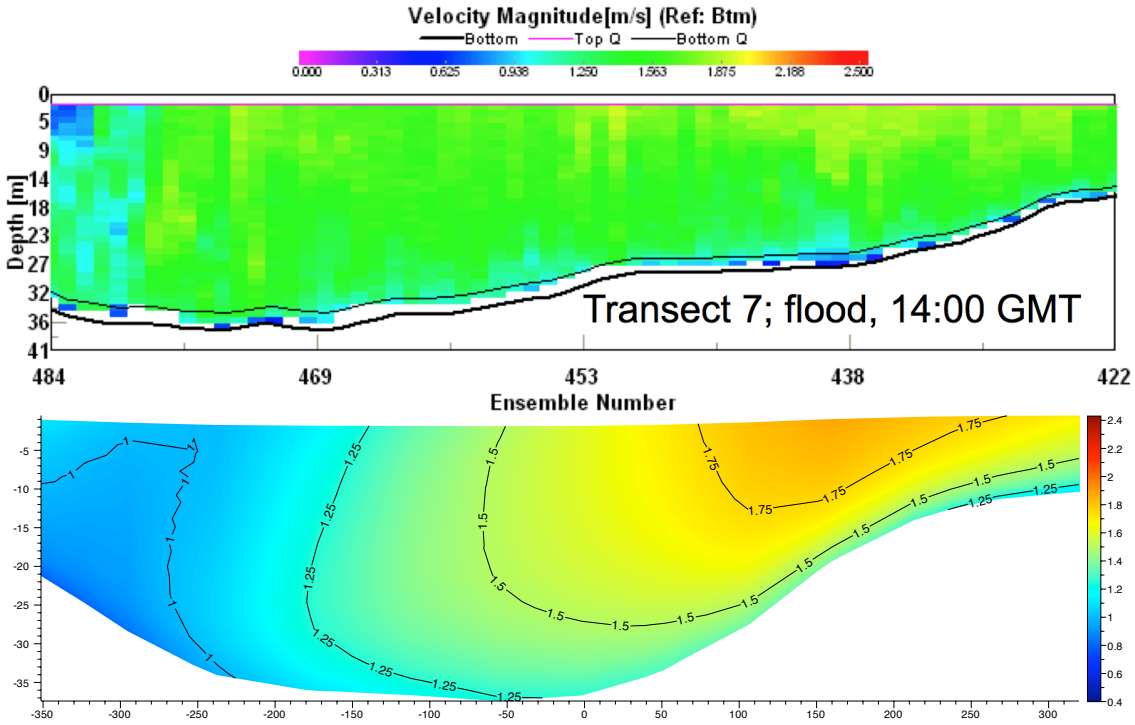

Figure III-12a: Velocity (m/s) through Transect 7 during large spring flood tide. Upper: ADCP-measured. Lower Model-computed.

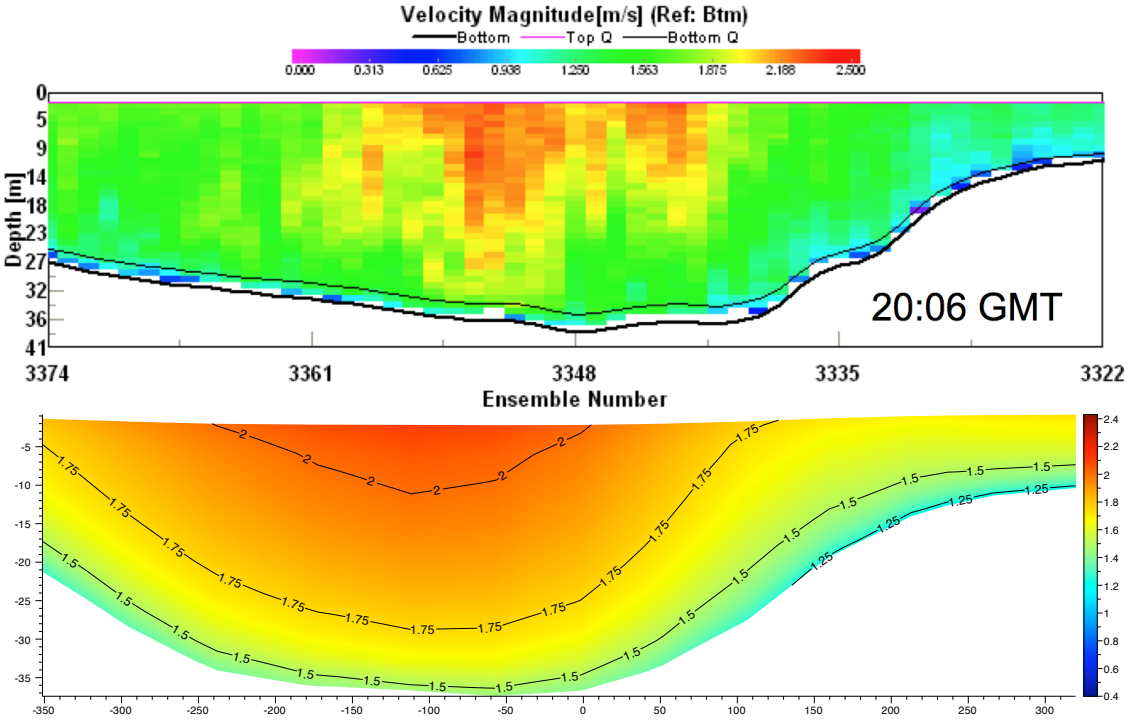

Figure III-12b: Velocity (m/s) through Transect 7 during large spring ebb tide. Upper: ADCP-measured. Lower Model-computed.

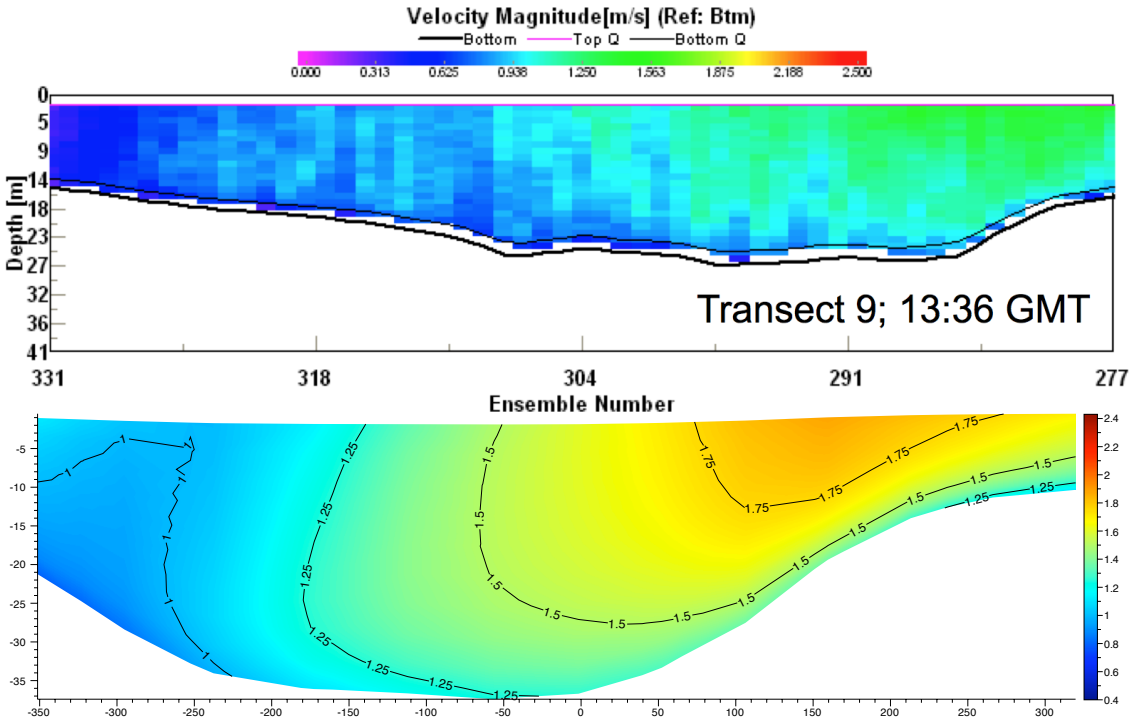

Figure III-12c: Velocity (m/s) through Transect 9 during large spring flood tide. Upper: ADCP-measured. Lower Model-computed.

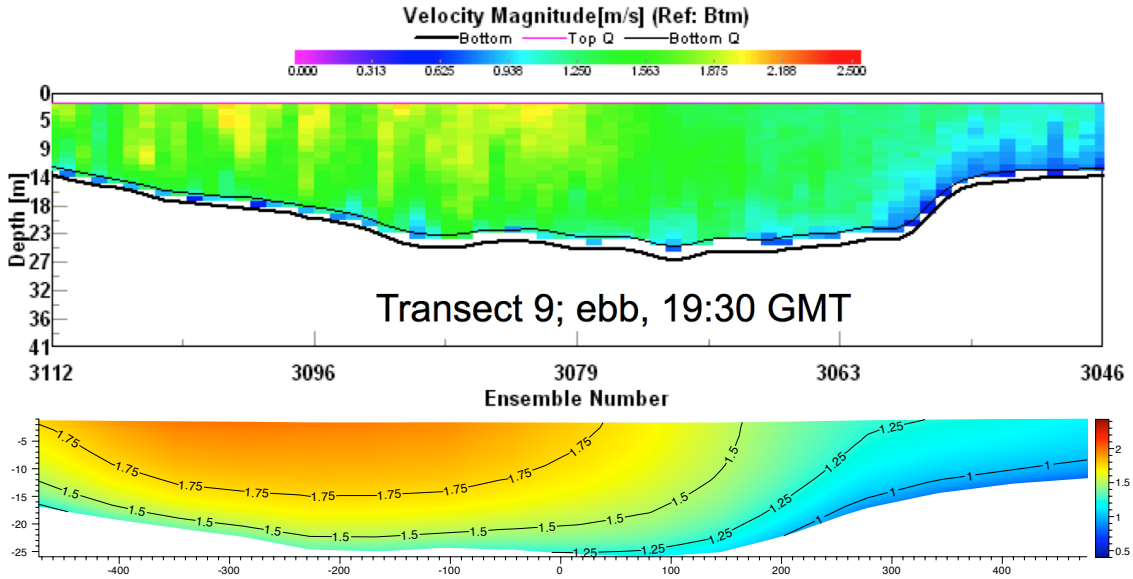

Figure III-12d: Velocity (m/s) through Transect 9 during large spring ebb tide. Upper: ADCP-measured. Lower Model-computed.

Impact Experiments

Setup

To drive the sediment model an initial distribution of grains must be prescribed. Due to the heterogeneity of the substrate, there were not sufficient measurements in the region to derive the distribution directly from observations. For this reason we chose to let the model sort the grains under tidal forcing. A two-layer bed was initialized with equal distributions of eight grain sizes ranging from coarse silt ($\phi = 4.5$) to coarse granule ($\phi = -2.5$) in the Wentworth scale (Table III-2). All sediments are treated as non-cohesize and the larger sediments (very coarse sand to granule) are generally transported as bedload . Although larger size sediments have been observed (cobble, boulders), much of this would be heterogenous, glacial in origin, and unlikely to be highly mobile at the time scales of our interest given the shear stresses predicted by the model. Parmeterizing the effects of such scattered roughness elements on bed stress at the larger model scale is an active area of research. The model was forced by tides for a period of sixty days at which point the majority of discrete bed points in the model had reached a quasi-steady state distribution. The resulting distribution of mean surficial grain size compares well with spatial distribution derived from the US Seabed (Poppe et al., 2003) database and measurements acquired by the SMAST Coastal Systems Lab with support from this project (Fig III-13). Coarser sediments are present in the main channel and along the flanks in areas of high stress. Finer sediments are present along Wasque shoals and where the circulation and sediment availability allow for finite fractions to persist. The resulting spatial distribution of fractions of the eight size classes is saved and used to initialize the bed in the ISE experiments described below.

Class	Grain Size(mm)	ϕ	Settling Velocity (mm/s)	Critical Shear Stress (N)	Porosity
Coarse Silt	.04	4.5	1.2	.1	0.5
Very Fine Sand	.09	3.5	4.73	.133	0.5
Find Sand	.18	2.5	17.64	.165	0.5
Medium Sand	.35	1.5	47.21	.213	0.5
Coarse Sand	.71	.5	90.32	.340	0.5
Very Coarse Sand	1.41	-.5	142.8	.740	0.5
Coarse Granule	2.83	-1.5	210.3	1.92	0.5
Granule	5.66	-2.5	301.63	4.70	0.5

Table III-2: Sediment Classes and Characteristics for ISE Impact Studies

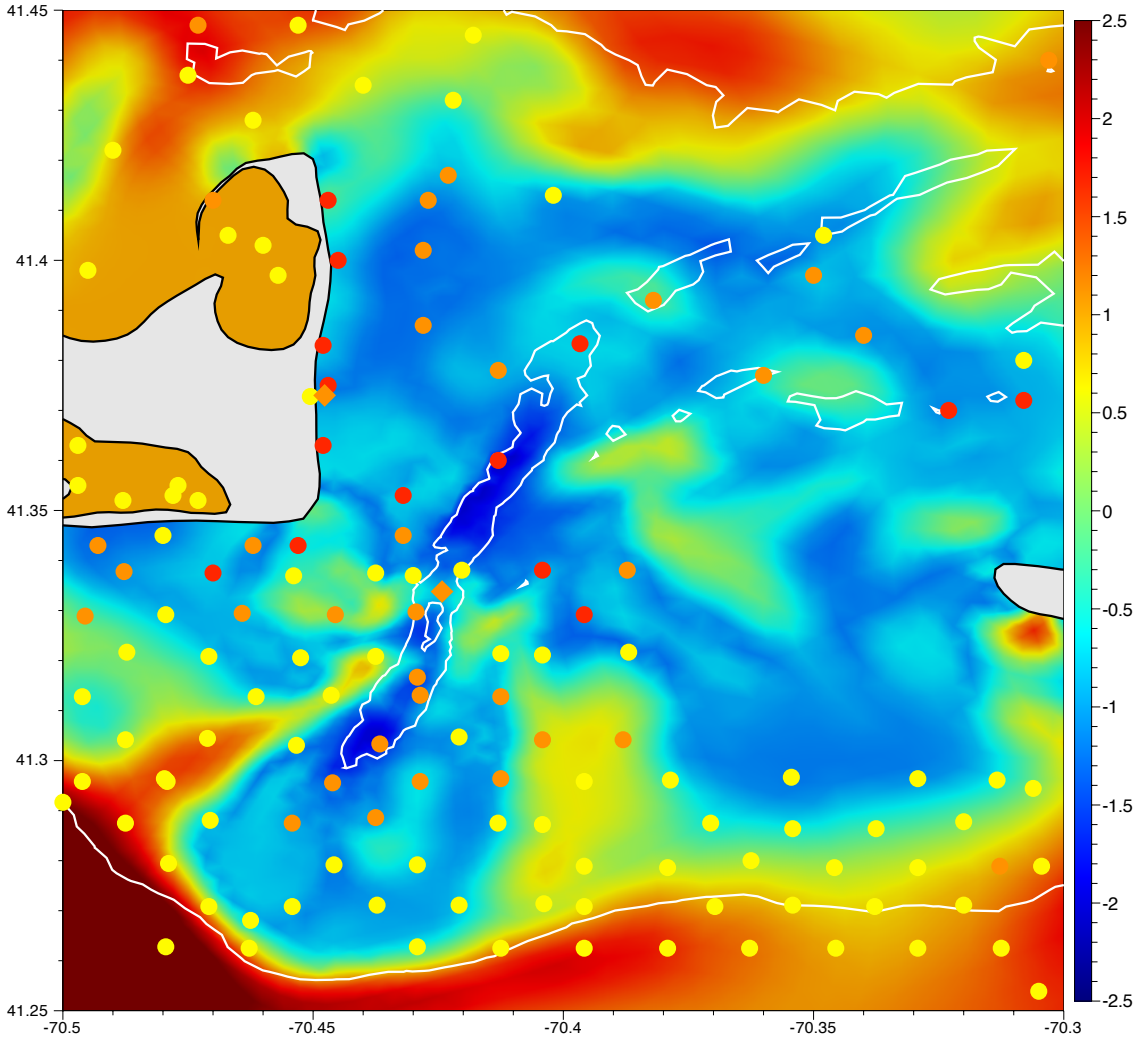

Figure III-13: Surficial median grain size distribution (phi) used to initialize the model impact experiments with USGS Seabed (circles) and SMAST CSP (diamonds) measurements for comparison (red = gravel, orange = gravelly sediment, yellow = sand). 15-m and 35-m isobaths are included for reference.

Turbine layout and sizing was based on a preliminary assessment for tidal energy in Muskeget Channel by the Ocean Renewable Power Company (ORPC, 2010). Using velocity distributions from ADCP transects acquired by the SMAST Coastal System Program in combination with channel bathymetry, ORPC determined the optimal layout for their crossflow turbines for transects 6-9 (Table III-3). Their basic turbine design allows for efficient site-specific configuration. These configurations were used to establish the spatial distribution of parameters in Eq III-1 within the FVCOM mesh. The power coefficent C_p was determined using the ratio of reported rated power to freestream tidal power through the cross-sectional area of the housing (ORPC, 2010).

Transect	Baseline Config	# Configs	Total width [m]	Total area [m^2]
6	2-TGU	6	166	1412
7	4-TGU	9	249	4238
8	4-TGU	5	138	2354
9	2-TGU	5	138	1177

Table III-3: Turbine subgridscale parameterization for Impact Studies.

Power Computations

Fields for the turbine subgridscale parameterization were extracted from the hourly-archived model data to reconstruct the installation power. Figure III-14 (upper panel) shows a comparison of the power (MW) for both the coarse grid (mtm-4, dashed lines) and fine grid (mtm1, solid lines) solutions for installations on transects 6-9 using M_2 tidal forcing. In comparison with the fine grid, the coarse grid does remarkably well capturing the power generation and is much more efficient (Table III-1).

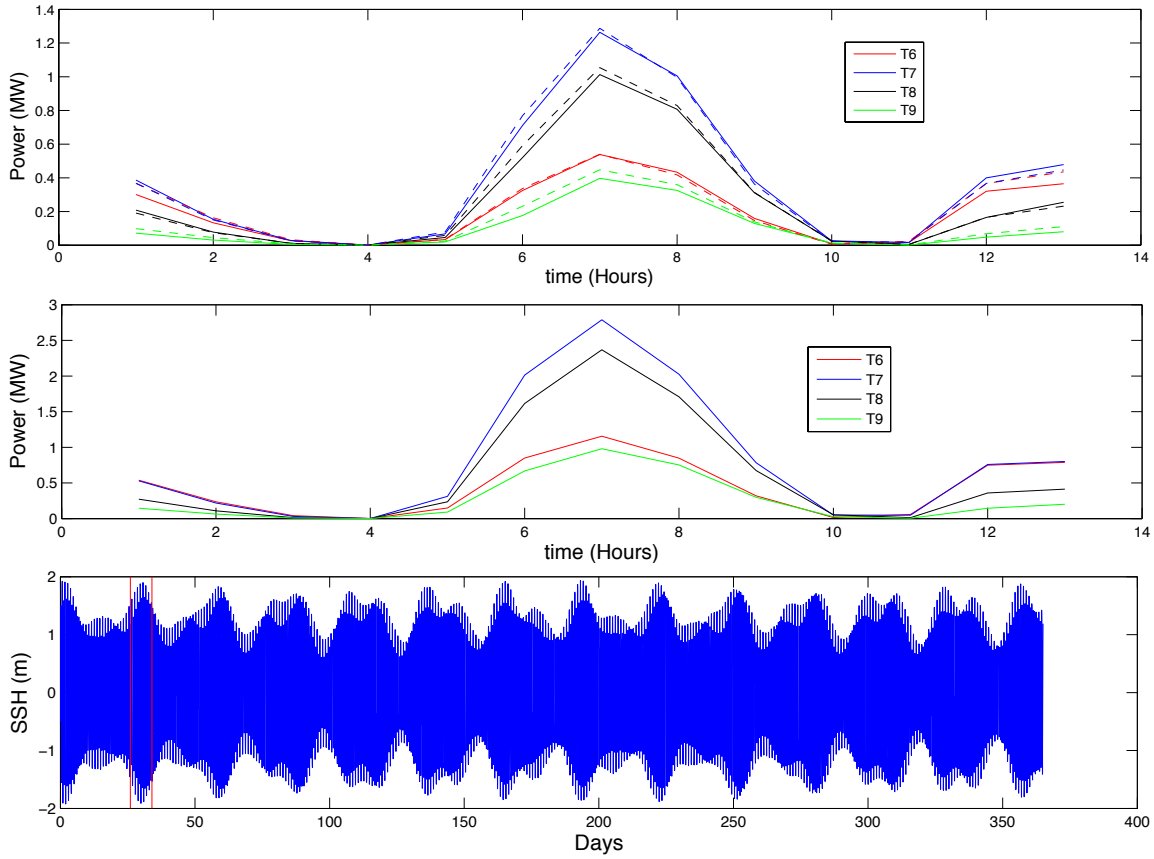

Figure III-14: Upper: Power captured by device array through transects 6-9 forced by M_2 tidal forcing using MTM1 (solid line) and MTM4 (dashed line) models. Middle: Power captured by device array through transects 6-9 forced by the dominant six components of tidal forcing using MTM4. Lower: sea surface elevation (m) at the open boundary for model forced by six components of tidal forcing. Red bars show time frame containing tidal cycle for power curves in central panel.

Power curves for the coarse grid (mtm4) for a solution forced by the six major tidal components are shown in Figure III-14 (center panel). These curves was extracted over a larger spring tide (red zone, Fig. III-14, lower panel) which would be comparable to the large spring tide during which the ADCP data was acquired by the SMAST Coastal Systems Program. The peak power occurs during ebb tide and is good agreement with the estimates made by ORPC based on the ADCP data. As these estimates required obtaining an average observed velocity along a transect and rounding to the nearest knot to apply the rated power, it would not be possible to get perfect agreement. Installations along the intermediate transects (7,8) in the deeper sections are able to provide the most power while the northernmost (6) and southernmost (9) sections have decreased potential due to the limited depth of water. It should be noted that in the subgridscale parameterization, it is assumed that the devices are always oriented perfectly normal to the flow. The flow through the northern portion of Muskeget is more or less rectilinear so it is possible to meet this condition with a fixed orientation device. At the southernmost transect (6), there is more appreciable deviation in flood and ebb direction which would result in a decrease in efficiency in a fixed-orientation device.

Sea Surface Height Perturbation

The turbine-induced modification to sea level is quite small. Muskeget is effectively a broad open channel and there is little lateral constraint. Reduced impacts on sea level are an advantage of using a TISEC approach to energy extraction vs. a head-based approach such as a barrage. In the region of Muskeget Channel as defined by the 15-m isobath, the change in sea surface height (SSH) induced by the installations is roughly 3 mm (Fig. III-15). The head builds up against the device and relaxes downstream (Fig. III-16). The adverse slope in the upstream section (~1.5e-6 m/m) represents a pressure gradient with a driving force on par with a local wind blowing at 15 knots in 30-m water. This adverse pressure gradient is responsible for the relative decrease in velocity upstream of the turbine (Figure III-17).

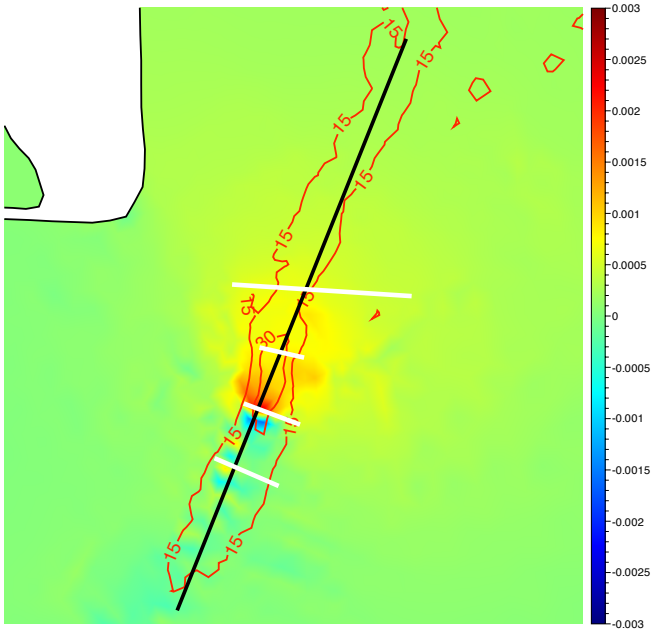

Figure III-15: Difference in model-computed free surface height between Transect-8

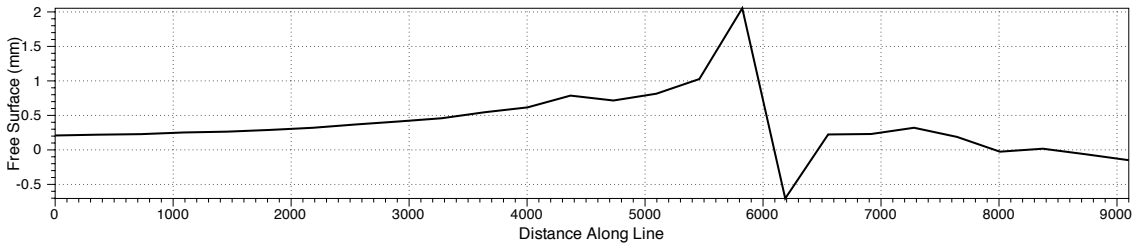

Figure III-16: Difference in model-computed free surface height (mm) along the main channel from North to South between a simulation of Transect-8 installation and natural conditions (ref: black line in Figure III-15). The approximate location of the installation along the transect is at x=6000.

Vertically-Averaged Velocity and Bed Stress Perturbation

The extraction of momentum by the turbines modified the velocity field in region around the turbine. This is best examined by subtracting the natural (no turbine) flowfields from the turbine-modified as the perturbations are generally small compared to the background flow. A momentum deficit forms in the wake (Fig. III-17, left panels), extending downstream. During ebb, the velocity defect associated with energy extraction is roughly 5 cm/s. The velocity magnitude is also reduced upstream of the turbine but the magnitude of the impact is less than 1 cm/s. In association with the decreased velocities and reduction of momentum is a lateral pressure gradient which drives the flow around the turbine which can be thought of as a partial fence in the water column. The velocity is increased on the flanks of the Channel by roughly 2 cm/s. The modification to the vertically-averaged flow on flood (Fig. III-17, lower left) is spatially similar with a reduced magnitude as the Channel is strongly ebb dominant. Associated with the modifications to the velocity field are perturbations to the bed stress which generally scales as the square of the velocity. During ebb the model-computed bed stress for an installation at Transect 8 is decreased in the main channel by roughly 0.25N and increased along the flanks the Channel by rough 0.1N. On flood tide, a similar pattern appears but the magnitude of bed stress perturbations is reduced accordingly. Spatial distribution of bed stress perturbations for installations at other transects follows the same general pattern with reduced stresses in the channel and enhanced stresses along the edges. In our sediment simulations, it is the current-induced bed stresses that drive the sediment model and thus changes in sediment fluxes are induced solely by pertubations.

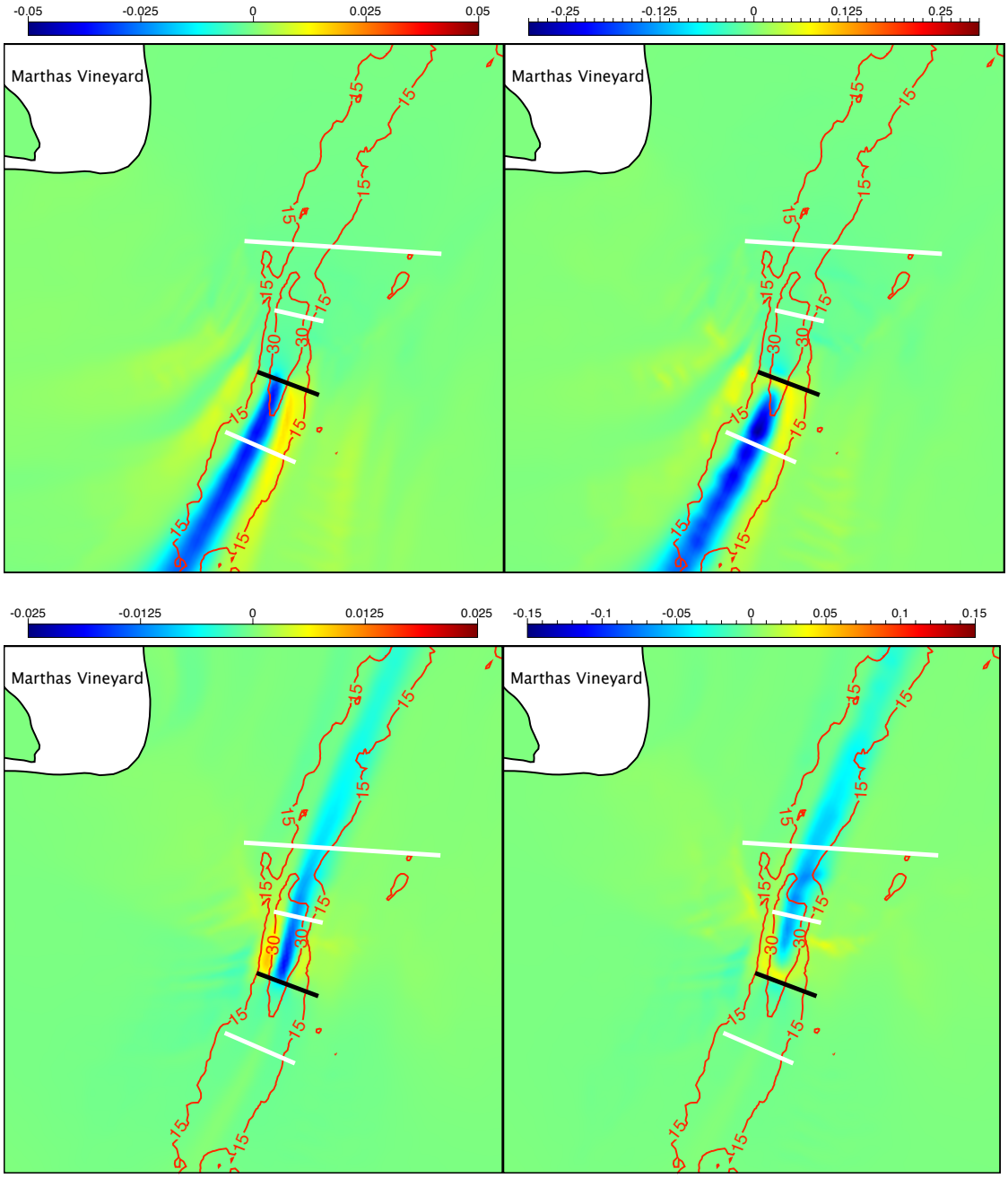

Figure III-17: Upper Panels: difference in model-computed vertically-averaged velocity magnitude (m/s) and bed stress (N) during ebb for simulations with turbine installation at transect 8 and natural conditions. Lower Panels: difference in model-computed vertically-averaged velocity magnitude (m/s) and bed stress (N) during flood for simulations with turbine installation at transect 8 and natural conditions.

Large Scale Modification to Bed Height

In an initial sediment and erosion (ISE) experiment, hydrodynamic and sediment transport computations are made based on the assumption of an invariant bed topography. Such an approach is widely used as the computational effort is constrained and the difficulties associated with the implementation and solution of an evolution equation for the bed height are avoided. However, since the morphodynamic feedback is not included in an ISE model, the results must be interpreted with caution. The net erosion/deposition predicted by the model are useful for evaluting the spatial variation in the initial adjustment of the bed but will not be accurate over the long term where the resulting bathymetric changes feed back to the flowfield. Such morphodynamic modeling was beyond the scope work in this project but would be a logical next step in future efforts. The experiments here were initialized using a spatial distribution of sediment fractions with median size shown in Figure III-13. The bed was then allowed to evolve based on net deposition and erosion of the eight sediment classes for 30 days under M_2 forcing both with and without turbines. We focused here on the single tidal consitituent as it can be more easily upscaled through a number of tidal cycles. By including all six constituents, approximately a full year is needed to experience the entire tidal range.

The relative change in bed heights (m) between turbine-modified and natural simulations forced by M_2 tides is shown in Figure III-18. These fields should not be interpreted as actual accretion or erosion, rather a net accretion or erosion relative to evolution of the bed in natural flow conditions. In all three cases there is a net positive change in the bed height which is consistent with effects of the turbines as energy needed to erode and trasnsport sediment is being removed from the system. This net accretion was approximately 15% of the total absolute change in model computed bed thickness for all four turbine installations. In all four cases the spatial distribution of relative changes follows the basic pattern of changes in bed stress resulting from the momentum removal (Figure III-17). However sediment erosion and deposition is more closely related to the divergence of the bed stress. For installations at all sites there is a positive change in bed thickness in the main channel with a negative change on the flanks of the Channel. Over the thirty day period this net bed change is approximately 5-10 cm at the central transects and 2-5 cm at the northern (transect 9) and southern (transect 6) installations. The total volume associated with the relative change in bed thickness within the domain shown in Figure III-18 is shown in Figure III-19. It is seen to be monotonically related to the power extracted by the devices. As these experiments were conducted with M_2 forcing only, the actual installations would have larger power output (roughly 220%) and accordingly, larger relative changes in bed heights over a given period.

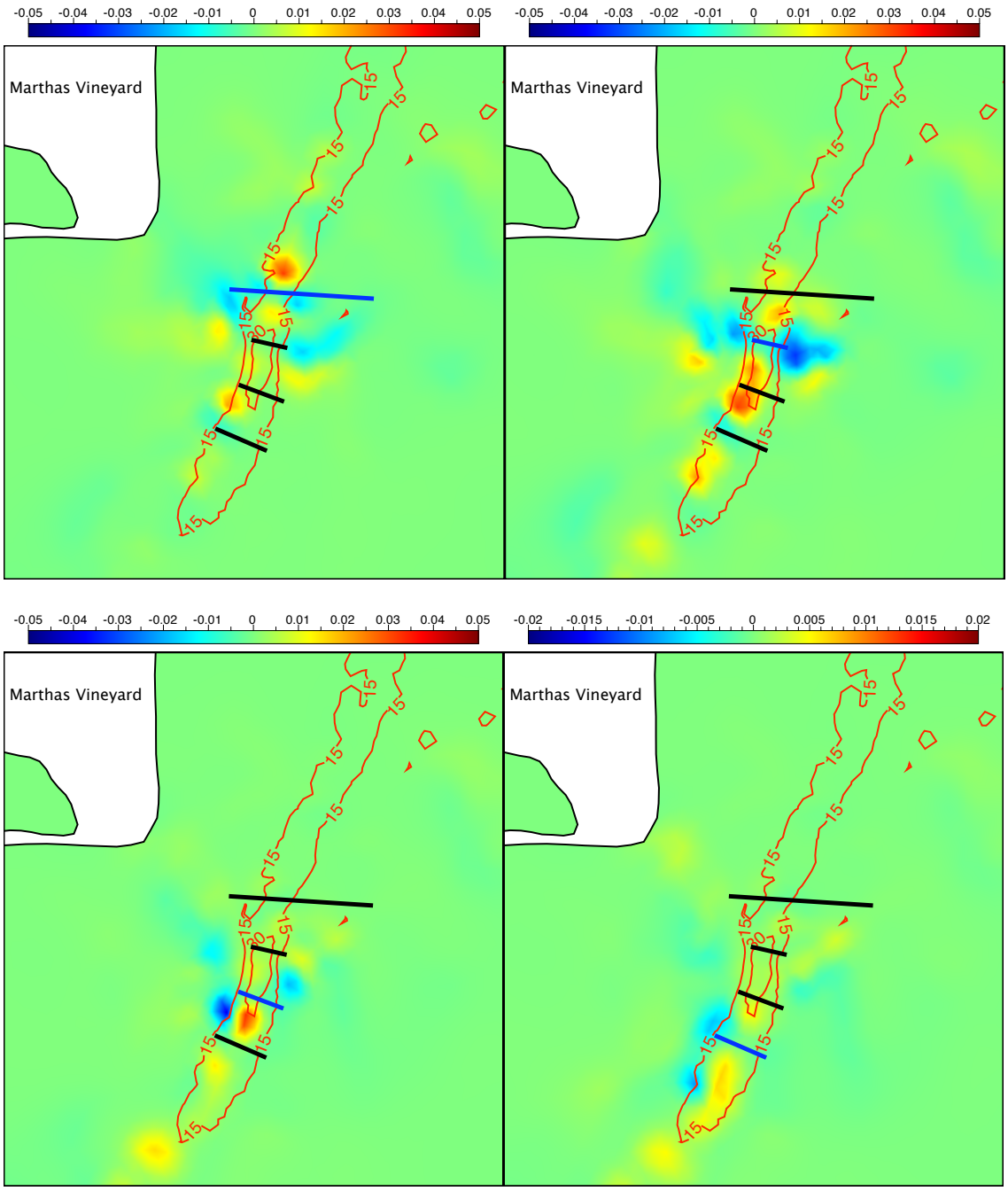

Figure III-18: Differences in model-computed and natural bed thickness (m) over a 30-day period for a simulation driven by M_2 tides for installations at four different transects. Clockwise from Upper Left: Transect 6, Transect 7, Transect 8, Transect 9 (ref: blue line is transect of turbine installation).

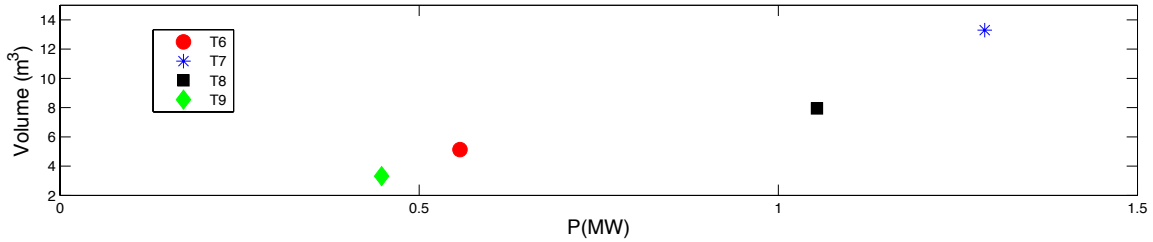

Figure III-19: Total absolute difference in bed volume over 30 days in the region enclosed in Figure III-19 between simulation with turbines and natural flow (m^3) vs the max power captured by the turbine array (MW). Simulations here used M_2-forcing only.

Modification to Sediment Fluxes

Fluxes of sediment through the Channel were examined along three transects: one north of the area of interest in energy extraction, one south, and one intersecting the primary area of interest between ADCP survey transects 7 and 8 (Fig. III-20). During flood the model-computed sediment loads are on the order of 1 kg/(m-s) at the central and northern transects with weaker values along the southern transect indicating a convergence of sediment from the east and west flanks of the Channel (Fig. III-20). During ebb, values are approximately 50% higher corresponding to the greater shear stress (Fig. III-21) deriving from the ebb-dominant flow in the nearfield of the main channel (Fig. III-2).

The effect of energy extraction can be evaluted by subtracting the instantaneous sediment fluxes computed with the subgridscale turbine model in place by the fluxes computed in natural conditions (Fig. III-20,III-21). Flux perturbations are O(10) g/(m-s) corresponding to approximately 1% of the natural fluxes.

During flood, the perturbations to the transect fluxes due to augmentations in the device-influence flowfield are most significant along the central and northern transects where the along-transect distribution reflects the variations in bed height observed during the sediment experiments. The largest defects in the flux occur in the main channel, particularly where a flux transect is proximal to the installation in the downstream direction (e.g. the influence of an ADCP transect 9 installation on the north flux transect). On the edge of the channel the fluxes are enhanced due to the local increase in bedstress. Transect 9 installation is seen to have only a nominal influence of the load. This is due primarily to the reduced amount of energy harvested at this site in comparison to the proposed installations at transect 7 and 8.

Ebb tide flux augmentations are essentially the reverse of flood with flux defects occurring in the channel and flux enhancements on the flanks except with greater magnitude. The largest along-channel flux defect, on the order of 0.05 kg/(m-s) is observed in the central flux transect just downstream of the transect 7 installation.

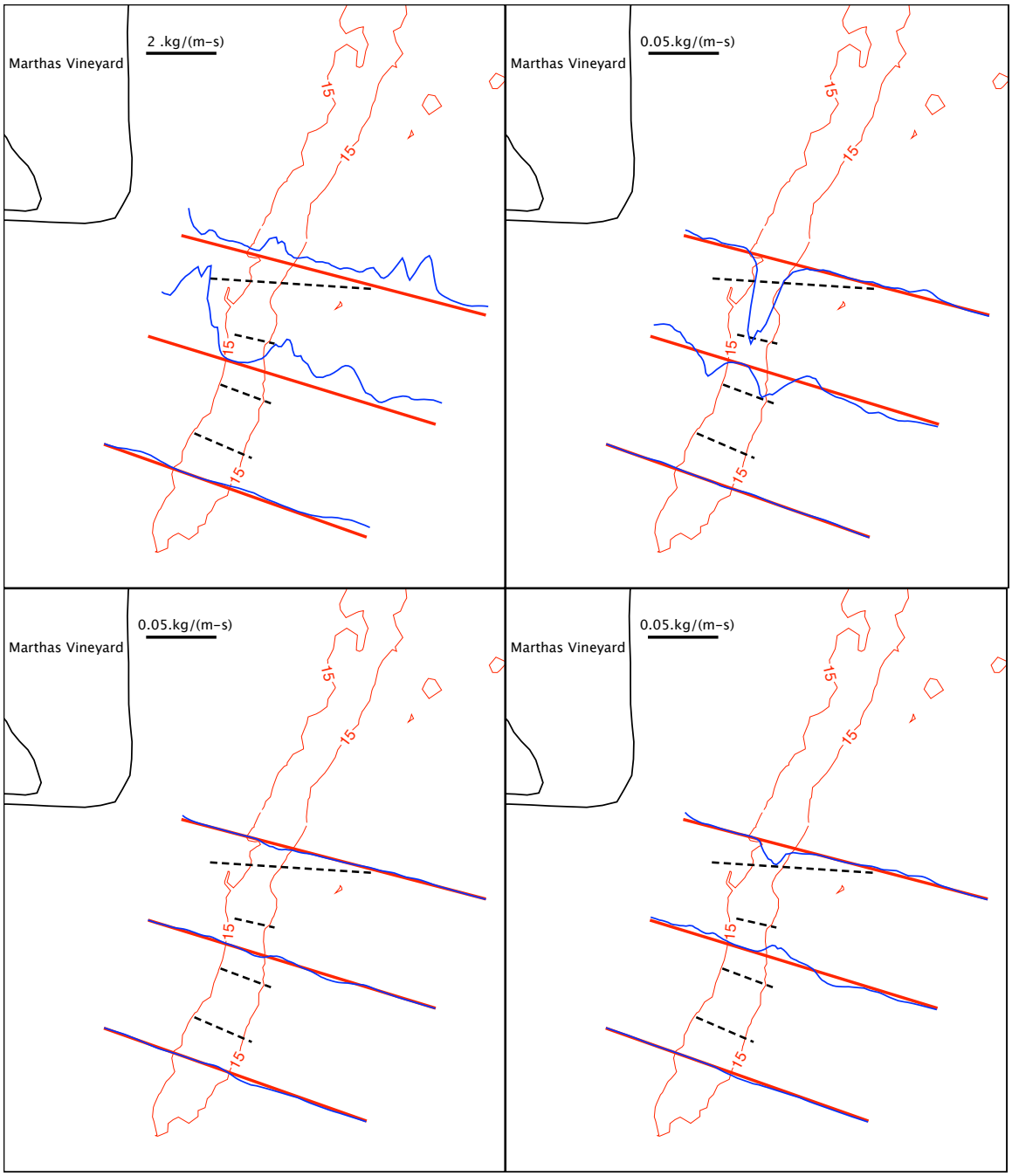

Figure III-20: Total sediment (bedload + suspended load) fluxes across three transects (red lines) during flood tide for a simulation in the mtm-4 domain driven by M_2 forcing. Clockwise from upper left: Natural fluxes, (ii) difference between installation-modified and natural fluxes for an installation at ADCP transect 7 (upper right); difference between installation-modified and natural fluxes for an installation at ADCP transect 8 (lower right); and difference between installation-modified and natural fluxes for an installation at ADCP transect 9 (lower left). ADCP transects 6-9 (black dashed lines) and 15-m isobath shown for reference

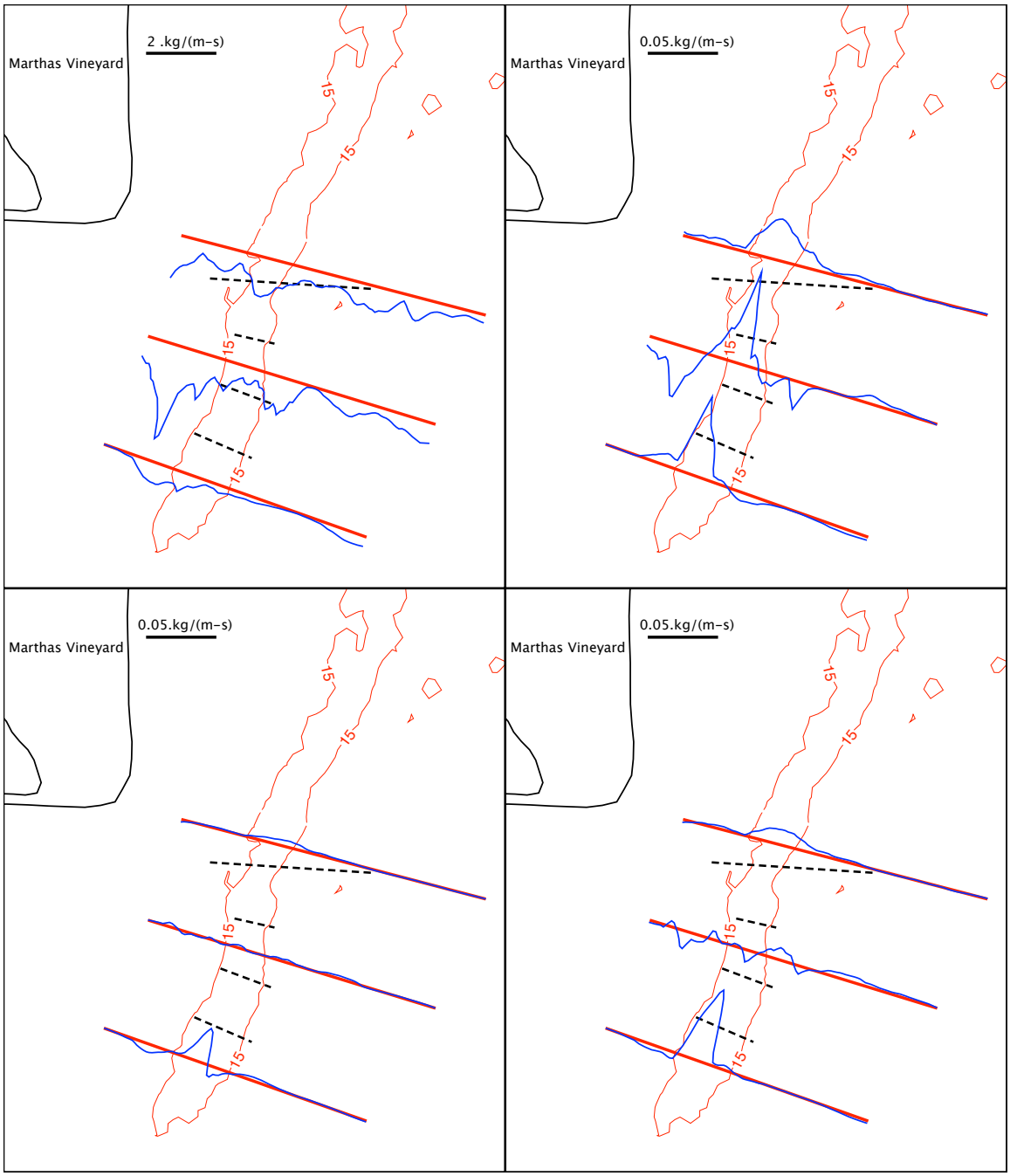

Figure III-21: Total sediment (bedload + suspended load) fluxes across three transects (red lines) during ebb tide for a simulation in the mtm-4 domain driven by M_2 forcing. Clockwise from upper left: Natural fluxes, (ii) difference between installation-modified and natural fluxes for an installation at ADCP transect 7 (upper right); difference between installation-modified and natural fluxes for an installation at ADCP transect 8 (lower right); and difference between installation-modified and natural fluxes for an installation at ADCP transect 9 (lower left). ADCP transects 6-9 (black dashed lines) and 15-m isobath shown for reference

SUMMARY

a. USGS SWATH bathymetry survey data was used to evaluate the characteristics of large scale bedforms in the main Muskeget Channel and outlying regions. The asymmetry of these bedforms indicate they are generated by residual currents and their orientation is consistent with the directionality of model-predicted tidal residual.
b. The proposed cable connection to Marthas Vineyard via Chappaquiddick directly interesects an area of medium sized bedforms of O(1m). Dredge depth would have to be carefully evaluated.
c. The bedform characteristics of Muskeget Channel and vicinity are in the range of empirical relationships for dynamic bedforms derived from other high energy sites.
d. A hydrodynamic model was developed to examine impacts of energy removal in Muskeget Channel. The model was validated using local tidal harmonics as well as comparisons of cross transect velocity with ADCP studies during large spring tides. The model captures well the sea surface elevation as well as the spatial complexity and magnitude of the velocity in the Channel as well as the strong flood-ebb asymmetry.
e. A spatial map of discrete grain fractions was developed by running a coupled hydro-sediment model with 8 grain sizes and letting the bed reach a quasi-steady state. The grain sizes reflect well the large scale regional heterogeneity as determined from core samples which range from sands to gravel.
f. Model-computed perturbations to sea level due to proposed installations outlined by ORPC indicate changes on the order of several mm extending several km in all directions. Sea surface slope modifications are roughly 1.5e-6 m/m. Given that Muskeget draws tidal power from phase differences rather than a constriction, this limited impact on sea surface height is not surprising.
g. Tidal kinetic energy extraction is associated with reduced velocities in the channel and enhanced over the flanks. Model computed velocity and stress defects in the channel during ebb are on the order 5cm/s and 0.25N respectively. On the flanks the velocity and bedstress are enhanced by ~2cm/s and 0.1N respectively.
h. Consistent with the spatial distribution of changes in the bed stress, the erosive potential is reduced in the channel upstream and downstream of the device and increased on the flanks of the channel adjacent to the location of installation. Over a 30-day period, localized areas with net changes in bed height of ~5cm are expected as the topography adjusts to the device-augmented flow conditions.
i. Augmentations to instantaneous fluxes on the order of 0.05 kg/(m-s) are observed for installation-augmented flow conditions. Flux defects are maximum in the main channel downstream of the turbine installation.

REFERENCES

Chen, C., H. Huang, R.C. Beardsley, Q. Xu, R. Limeburner, G.W. Cowles, Y. Sun, J. Qi, H. Lin, 2011. Tidal dynamics in the Gulf of Maine and New England Shelf: An application of FVCOM, Journal of Geophysical Research, in press.

Chen, C, R. C. Beardsley and G. Cowles, (2006). An unstructured grid, finite-volume coastal ocean model (FVCOM) system. Special Issue entitled "Advance in Computational Oceanography", *Oceanography*, **19**(1), 78-89.

Chen, C., H. Liu, and R. Beardsley, (2003) An unstructured grid, finite-volume, three-dimensional, primitive equations ocean model: Application to coastal ocean and estuaries. Journal of Atmospheric and Ocean Technology, 20 (1), 159–186.

Cowles, G**.**, (2008), "Parallelization of the FVCOM Coastal Ocean Model", *International Journal of High Performance Computing Applications 22(2) 177-193*.

Denny, J.F., Danforth, W.W., and Signell, R., (2012), Swath Bathymetric Data collected within Muskeget Channel, MA. USGS Open-File Report, 2012-XXXX (in prep).

Kobayashi, M. H., J. M. C. Pereira and J. C. F. Pereira (1999). A conservative finite-volume second-order-accurate projection method on hybrid unstructured grids. *J. Comput. Phys*., 150, 40-45.

Madala, R. V., and S. A. Piacsek (1977). A semi-implicit numerical mode for baroclinic oceans, *J. Comput. Phys*., 23, 167–178.

Meyer-Peter, E., Müeller, R., (1948). Formulas for bedload transport. In: Report on the 2nd Meeting International Association Hydraulic Structure Research. Stockholm, Sweden, pp. 39–64.

ORPC, (2010). Preliminary Tidal Energy Assessment for Muskeget Channel. Technical Report prepared for Harris, Miller, Miller, and Hanson Inc. for the Town of Edgartown, MA, 12 pp.

Poppe, L.J., Paskevich, V.F., Williams, S.J., Hastings, M.E., Kelley, J.T., Belknap, D.F., Ward, L.G., FitzGerald, D.M., and Larsen, P.F. (2003). Surficial Sediment Data from the Gulf of Maine, Georges Bank, and Vicinity: A GIS Compilation. U.S. Geological Survey Open-File Report 03-001.

Réthoré, P.-E., Sørensen, N.N., and Bechmann, A. (2010). CFD Model of wind turbine wake in atmospheric turbulence using body forces. *Proceedings of the IEA Offshore Wake Workshop*, Risø, 2009.

Warner, J. C., Sherwood, C. R., Signell, R. P., Harris, C. K., and Arango, H. G. (2008) Development of a three-dimensional, regional, coupled wave, current, and sediment- transport model. Computers & Geosciences, 34, 1284–1306